

**Multi-phase competition in quantum XY pyrochlore
antiferromagnet CdYb_2Se_4 : zero and applied magnetic field study**

K. Guratinder

*Laboratory for Neutron Scattering and Imaging,
Paul Scherrer Institute, CH-5232 Villigen, Switzerland and
Department of Quantum Matter Physics,
University of Geneva, CH-1211 Geneva, Switzerland*

Jeffrey G. Rau

Max-Planck-Institut für Physik komplexer Systeme, 01187 Dresden, Germany

V. Tsurkan

*Experimental Physics V, Center for Electronic Correlations and Magnetism,
University of Augsburg, D-86159 Augsburg, Germany and
Institute of Applied Physics, Academy of Sciences of Moldova,
MD-2028 Chisinau, Republic of Moldova*

C. Ritter

Institut Laue-Langevin, 156X, 38042 Grenoble Cédex, France

J. Embs and T. Fennell

*Laboratory for Neutron Scattering and Imaging,
Paul Scherrer Institute, CH-5232 Villigen, Switzerland*

H. C. Walker

*Rutherford Appleton Laboratory, ISIS Facility,
Chilton, Didcot, Oxon OX11 0QX, United Kingdom*

M. Medarde and T. Shang

*Laboratory for Multiscale Materials Experiments,
Paul Scherrer Institute, CH-5232 Villigen, Switzerland*

A. Cervellino

Swiss Light Source, Paul Scherrer Institute, CH-5232 Villigen, Switzerland

Ch. Rüegg

*Research Division Neutrons and Muons,
Paul Scherrer Institute, CH-5232 Villigen, Switzerland and
Department of Quantum Matter Physics,
University of Geneva, CH-1211 Geneva, Switzerland*

O. Zaharko*

*Laboratory for Neutron Scattering and Imaging,
Paul Scherrer Institute, CH-5232 Villigen, Switzerland.*

(Dated: November 1, 2021)

Abstract

We study magnetic behaviour of the Yb^{3+} ions on a frustrated pyrochlore lattice in the spinel CdYb_2Se_4 . The crystal-electric field parameters deduced from high-energy inelastic neutron scattering reveal well-isolated ytterbium ground state doublet with a weakly Ising character. Magnetic order studied by powder neutron diffraction evolves from the XY -type antiferromagnetic Γ_5 state to a splayed ice-like ferromagnet (both with $k=0$) in applied magnetic field with $B_c=3$ T. Low-energy inelastic neutron scattering identifies weakly dispersive magnetic bands around 0.72 meV starting at $|\mathbf{Q}| = 1.1 \text{ \AA}^{-1}$ at zero field, which diminish with field and vanish above 3 T. We explain the observed magnetic behaviour in framework of the nearest-neighbour anisotropic exchange model for effective $S = 1/2$ Kramers doublets on the pyrochlore lattice. The estimated exchanges position the CdYb_2Se_4 spinel close to the phase boundary between the Γ_5 and splayed ferromagnet states, similar to the Yb-pyrochlores suggesting an important role of the competition between these phases.

I. INTRODUCTION

The study of the family of rare-earth pyrochlores¹ of the form $R_2B_2O_7$, with R a trivalent rare-earth and B a non-magnetic transition metal, has unveiled a rich variety of correlated magnetic states with unconventional excitations. Examples include classical spin ices⁴ with emergent magnetic monopoles in $Ho_2Ti_2O_7$ and $Dy_2Ti_2O_7$, the physics of order-by-disorder in $Er_2Ti_2O_7$,^{2,3} an unusually broad continuum of excitations in the anisotropic ferromagnet $Yb_2Ti_2O_7$,^{2,3} and potential quantum spin liquid candidates in $Tb_2Ti_2O_7$,³ $Pr_2Hf_2O_7$ ⁵ and $Ce_2Zr_2O_7$ ⁶.

Many of these materials are well described by an effective spin-1/2 model with anisotropic exchange interactions. This effective spin-1/2 arises from the presence of a large crystal-electric field (CEF) splitting, isolating the ground doublet from the higher lying excitations⁷. The low energy physics of these effective spin-1/2 models can exhibit strong quantum effects; this is especially true for trivalent ytterbium compounds, where the (relatively) low total angular momentum ($J = 7/2$) allows for super-exchange interactions to induce quantum interactions, independent of the composition of the crystal field ground doublet⁸.

Interestingly, the same magnetic frustrated pyrochlore structure found in the $R_2B_2O_7$ compounds also arises in the *spinel*s with the composition TR_2X_4 (T=Cd, Mg, X=S, Se). However, unlike the usual pyrochlores where the local environment is a distorted cube of eight oxygens, in the spinels the rare-earth ion is surrounded by a near perfect octahedron of X ligands⁹. This structural difference distinguishes the spinels from the pyrochlores and allows for drastically different crystal field and exchange physics to arise, even for the same rare-earth element. As an example, while the Er-pyrochlores are XY magnets¹⁰, the Er-spinels exhibit dipolar spin ice physics^{11,12}. Consequently, this family of materials has attracted attention as providing new potential routes to explore some of the rich physics seen in the rare-earth pyrochlores in a new setting.

The ytterbium spinels, of the form TYb_2X_4 , in particular have attracted attention as possibly realizing highly frustrated quantum pyrochlore antiferromagnets^{8,13,14}. Earlier experimental analysis of TYb_2X_4 ¹³ found that all of the compounds order antiferromagnetically at $T_N \sim 1.6$ K – much lower than the estimated exchange scale of ~ 10 K, suggesting strong frustration. From the size of the local magnetic fields inferred from μ SR experiments, only a small static moment of $\sim 0.1 \mu_B$ was deduced. Antiferromagnetic order was directly ob-

served shortly afterwards¹⁴, with neutron diffraction detecting magnetic Bragg peaks with propagation vector $\mathbf{k}=0$, corresponding to a magnetic state in the Γ_5 irreducible representation¹⁶ with an ordered moment of $\sim 0.7\mu_B$. Together, these neutron and μ SR results suggest that the magnetic state has a dynamic character.¹⁴

In this article we present further experimental and theoretical exploration of CdYb_2Se_4 . We obtain more detailed information about the CEF using inelastic neutron scattering in combination with magnetization and susceptibility measurements. We then study how the magnetic order and spin dynamics evolve under the application of a magnetic field. We compare our findings with expectations for an effective spin-1/2 anisotropic exchange model on the pyrochlore lattice, motivated by recent results on the super-exchange mechanism in related breathing pyrochlore materials^{8,17}. From these considerations, we suggest that CdYb_2Se_4 may share some physics with the ytterbium pyrochlores $\text{Yb}_2\text{M}_2\text{O}_7$ (M=Ti, Sn, Ge), including proximity to a phase boundary between antiferromagnetic and ferromagnetic phases.

II. EXPERIMENTAL

A polycrystalline sample of 4.75 g of $^{114}\text{CdYb}_2\text{Se}_4$ was prepared by solid state synthesis from binary Yb and Cd selenides. The ^{114}Cd -isotope was used to reduce absorption in the neutron scattering experiments. The purity and crystal structure of the sample were checked by synchrotron x-ray powder diffraction on the Material Science beamline of Swiss Light Source SLS. The pattern collected with $\lambda=0.565475$ Å at room temperature is well fitted with the normal spinel structure with no site inversion. Tiny amounts of $\text{Yb}_2\text{O}_2\text{Se}$ and CdSe impurities (both below 1%) were detected.

Magnetic susceptibility and magnetization were measured in the temperature ranges 0.5 K - 4 K and 1.8 K - 400 K in applied magnetic fields up to 7 T using a Magnetic Properties Measurement System superconducting quantum interference device (SQUID) magnetometer and a Physical Properties Measurement System, both from Quantum Design.

High-energy time-of-flight inelastic neutron scattering (INS) measurements were performed on the MERLIN spectrometer¹⁸ at ISIS. The powder sample, contained in an aluminium can in an annular geometry, was inserted into a closed cycle refrigerator. An incident neutron energy of $E_i=150$ meV and chopper frequency 450 Hz were used on cooling and then

a setup with $E_i=50$ meV and chopper frequency of 500 Hz was chosen to record data at 8 K and 295 K. We used the McPhase program¹⁹ to extract the crystal electric field parameters from the measured spectra.

Neutron powder diffraction (NPD) experiments in zero and applied magnetic fields were performed on the DMC diffractometer at SINQ and on the high-flux diffractometer D20 at ILL ($\lambda=2.41$ Å). We present here the results from D20. The polycrystalline sample was mixed with deuterated ethanol and methanol solution and placed in a double-wall Cu cylinder with inner and outer diameters 8 and 10 mm. The sample was then mounted in an ^3He insert in a 6 T magnet and cooled down to 0.45 K. Special care was taken to have zero applied field for the first cooling of the sample by demagnetizing the magnet before the usage. The Fullprof suite²⁰ was used to refine difference diffraction patterns between an ordered state at a given field B at 0.45 K and the paramagnetic state at $T=2.5$ K measured in zero field.

Low-energy inelastic neutron scattering measurements were performed on the FOCUS spectrometer at SINQ. A double-wall Cu-can with the sample was inserted in a dilution refrigerator and a 10 T magnet. The base temperature of 0.1 K was reached. Two instrumental setups were used - with $E_i=10.4$ meV (with elastic resolution $\delta E_0 \approx 0.8$ meV) and with $E_i=3.7$ meV ($\delta E_0 \approx 0.35$ meV). Empty can and vanadium corrections were performed.

III. RESULTS

A. INS measurement of CEF excitations

The INS spectra measured on MERLIN ($E_i=50$ meV) contain two dispersionless excitations at 28.33(2) meV and 31.07(2) meV, which have highest intensity at low momentum transfer $|\mathbf{Q}|$ and at low temperature (Fig. 1). Therefore we attribute them to CEF transitions. These observations agree with the four doublet level scheme expected for Yb^{3+} -ion in chalcogenide spinels.^{8,13} The ground state (GS) doublet is separated by a significant gap of ~ 30 meV from two of the three higher lying doublets.

The excitation at 18.8(7) meV is pronounced at high Q and at high temperature. By comparison with measurements of an empty aluminium can (not shown here) we attribute this signal to aluminium phonons.

We did not observe any high-energy excitations with the $E_i=150$ meV setup, suggesting that the transition to the highest lying CEF level has very small intensity, below the experimental sensitivity.

B. Bulk measurements

The inverse magnetic susceptibility, χ^{-1} , of our polycrystalline sample (Fig. 2) is in accordance with the published results.^{13,14} The temperature dependence χ^{-1} can be divided into four regions: the $200 \text{ K} < T < 400 \text{ K}$ high-temperature (HT) linear regime, $20 \text{ K} < T < 200 \text{ K}$ intermediate-temperature (IT) non-linear regime, $5 \text{ K} < T < 20 \text{ K}$ low-temperature (LT) linear correlated paramagnet regime and the strongly correlated (SC) regime $T < 5 \text{ K}$.

The HT linear regime is dominated by the susceptibility of the Yb^{3+} ions in their ground state, because the contribution of the two next excited states does not exceed 10%. We use this HT regime to corroborate the set of the CEF parameters deduced from INS.

The IT regime is not linear and the χ^{-1} slope changes significantly near 70 K, probably due to the development of spin correlations. Here it is complex to disentangle the CEF and exchange contributions to the susceptibility.

The LT linear regime is governed by exchange correlations between the Yb^{3+} ions with the $S = 1/2$ ground doublet. Fitting the susceptibility in the LT range to the Curie-Weiss law

$$\chi = \frac{C}{T - \Theta_{\text{CW}}},$$

yields the (nominal) Curie-Weiss temperature $\Theta_{\text{CW}} = -9.5(9)$ K and the Curie constant $C = 1.14(5)$. To get some idea of the exchange scale, we consider a nearest-neighbor Heisenberg model on the pyrochlore lattice where the implied exchange J would be given by

$$J/k_B = -\frac{3\Theta_{\text{CW}}}{zS(S+1)} \sim 7 \text{ K},$$

here k_B is the Boltzmann constant, $z = 6$ is the coordination number and $S = 1/2$. These values are consistent with those reported in Refs. 13 and 14.

From the temperature dependence of magnetic susceptibility we can also extract the effective magnetic moment

$$\mu_{\text{eff}}^2 = 3k_B/(N_A\mu_B^2)\chi T,$$

here μ_B is the Bohr magneton and N_A is Avogadro's number. In the LT range μ_{eff} is $3.03 \mu_B/\text{Yb}^{3+}$, while in the HT regime μ_{eff} saturates at $4.5\mu_B/\text{Yb}^{3+}$ (inset of Fig. 2), close to the (expected) free-ion value $4.54\mu_B$.

Magnetization measured at various temperatures in the 2 K - 300 K range (Fig. 3) does not saturate in a field of 7 T, reaching only $0.9 \mu_B/\text{Yb}$ at 2 K, likely due to the effects of the (relatively large) exchange interactions.

In the SC regime a pronounced anomaly in susceptibility at $T_N=1.8$ K signals the onset of long-range magnetic order (LRO). This LRO is fragile and the susceptibility $\chi = M/B$ differs below T_N when the sample is cooled in zero-field (ZFC) and in magnetic field (FC), even if the applied field is as small as 5 mT. Fig. 4, left shows the bifurcation of the susceptibility at T_N for the ZFC and the $B=5$ mT FC states. We estimate that the additional net ferromagnetic (F) component in the FC state is only $1.5 \cdot 10^{-5} \mu_B/\text{Yb}$. This bifurcation was observed also by Higo *et al.*,¹³ who suggested that the F-signal arises from domain walls formed below T_N . A similar FC/ZFC difference was also observed in $\text{Er}_2\text{Ti}_2\text{O}_7$ ²¹.

A significant change of the long-range order takes place at magnetic fields near $B_c=3$ T. The corresponding anomaly is well pronounced in the derivative dM/dB at 0.5 K compared to the monotonous behaviour at 1.75 K (Fig. 4 right). We interpret this observation as a field-induced crossover between different ordered states and use neutron powder diffraction to study the microscopic origin of this anomaly, as presented in Section III C.

C. Neutron diffraction in zero and applied magnetic fields

Our zero field neutron powder diffraction patterns (Fig. 5 left) are in agreement with results of Ref. 14. At the base temperature of 0.45 K we find magnetic intensity at the positions of the $\mathbf{k}=0$ propagation vector.²² No significant difference between the ZFC and 75 mT FC states is detected, which is not surprising as the inferred ferromagnetic component of the FC state seen in the susceptibility is tiny.

The more significant changes in diffraction patterns take place at higher fields (Fig. 5 right). The rise of intensity of two main magnetic reflections (0 0 2) and (1 1 1) starts to differ at $B_c=3$ T (Fig. 6), where the slope of intensity for the (2 2 0) reflection also changes (Fig. 6 inset). Due to the polycrystalline nature of the sample, we cannot disentangle B_c values for the different crystallographic directions. At 1.2 K the disparity happens at the

even lower field of ~ 2 T (not shown), which implies a tendency of lowering of B_c with temperature increase.

1. Low-energy excitations by neutron spectroscopy

Fig. 7 (top panel left) presents the low-energy excitations measured with the $E_i = 3.7$ meV setup on FOCUS at the base temperature of 0.1 K. The weakly dispersive band lying around $\hbar\omega = 0.72$ meV and the dispersive branches starting at $|\mathbf{Q}| = 1.1 \text{ \AA}^{-1}$ vanish at T_N and change with applied magnetic field, thus they are certainly magnetic. These excitations diminish with magnetic field and are not observed for $B > 3$ T (Fig. 7 (bottom panel left), where the anomaly in magnetization and neutron diffraction is also observed. No excitation could be detected for the setup with higher incoming energy $E_i = 10.4$ meV presumably due to the weakness of the signal.

IV. DISCUSSION

We first present the crystal-electric field scheme of Yb^{3+} based on our experimental findings and then discuss the model of cooperative phenomena and its agreement with the experimental results.

A. Crystal-electric field parameters

To characterize the crystal-electric field scheme of Yb^{3+} we used the CEF Hamiltonian:

$$H = B_0^2 O_0^2 + B_0^4 O_0^4 + B_3^4 (O_3^4 - O_{-3}^4) + B_0^6 O_0^6 + B_3^6 (O_3^6 - O_{-3}^6) + B_6^6 (O_6^6 - O_{-6}^6), \quad (1)$$

with the local quantization axis $\langle 111 \rangle$, Stevens operators O_n^m and the corresponding coefficients B_n^m .

The positions and intensities of the CEF excitations observed in the Merlin INS experiment were used to refine the CEF parameters with the simulated annealing algorithm of McPhase¹⁹. The parameter space which fits the data is rather wide. Incorporating susceptibility or magnetization data does not help to converge to a unique solution as only the HT regime can be used to fit the CEF parameters. To confine the fitting parameter space we decided to start simulated annealing from the CEF parameters estimated by Higo

TABLE I. The crystal electric field parameters for CdYb₂Se₄. The columns list the experimental (INS) E_{obs} and the calculated E_{calc} energies, the $|J_z\rangle$ components of the wave functions of the CEF levels, their g_{calc} and magnetic moment m_{calc} values. For comparison the ground state of CdYb₂S₄ (Ref. 13) is presented in the second row.

E_{obs} (meV)	E_{calc} (meV)	$ \pm\frac{7}{2}\rangle$	$ \mp\frac{5}{2}\rangle$	$ \pm\frac{3}{2}\rangle$	$ \pm\frac{1}{2}\rangle$	$g_{calc ,\perp}$	m_{calc} (μ_B)	
0	0	-0.268	0.882	0	± 0.388	3.67 2.11	1.37	
	0	-0.301	0.804	0	0.513	2.67	1.33	[13]
28.33(2)	28.34	0.848	0.407	0	∓ 0.339	4.93 1.56	1.55	
31.07(2)	31.37	0	0	1	0	3.42 0	0.99	
	63(3)	∓ 0.457	∓ 0.239	0	-0.857	2.18 4.00	1.75	

*et al.*¹³ from susceptibility data for CdYb₂S₄. This resulted in the following set of Stevens coefficients: $B_0^2 = -0.397$, $B_0^4 = 0.026$, $B_3^4 = 0.531$, $B_0^6 = 0.0001$, $B_3^6 = -0.005$, $B_6^6 = 0.003$ meV. Table I presents the resulting calculated energies and composition of the Kramers doublets, as well as their magnetic parameters.

The predicted wave function of the ground state is composed of the dominant $J_z = \pm\frac{5}{2}$ component and significant $J_z = \pm\frac{1}{2}$ and $J_z = \pm\frac{7}{2}$ contributions. It is weakly Ising with the effective g -factor components $g_{||} = 3.67$, $g_{\perp} = 2.11$ with respect to the local (111) axis. The calculated magnetic moment of the ground state is, thus $m = \frac{1}{2}\mu_B\sqrt{\frac{2g_{\perp}^2 + g_{||}^2}{3}} = 1.37 \mu_B/\text{Yb}$. The calculated energies of the two first excited levels fits the two observed INS excitations reasonably well. The highest doublet should be located at 63 meV according to our model, however due to a vanishingly small INS matrix element for the transition between the lowest and the highest doublets the intensity of this excitation is negligibly small.

Magnetization calculated for our CEF scheme using the SAFiCF code²³ gives good agreement to magnetization measured above the LT regime (Fig. 3). In the LT regime the single-ion model is no longer valid due to exchange-induced correlations and agreement is lost.

B. Cooperative phenomena

1. Magnetically ordered states from neutron diffraction

When determining the magnetic ground state and its evolution with applied magnetic field from neutron powder diffraction we followed the notations and symmetry analysis of Dalmas de Reotier *et al.*¹⁴ The distribution of magnetic intensity in our D20 experiment is identical to the one reported in Ref. [14] and our refinements confirm that the $\mathbf{k}=0$ magnetic order is described by the Γ_5 irreducible representation (IRR) with the basis vectors (BV) ψ_2 or ψ_3 . The magnetic moments are confined to planes perpendicular to the local $\langle 111 \rangle$ axes of the tetrahedron for both BVs, being coplanar for ψ_3 (along $\langle 110 \rangle$ axes) and noncoplanar for ψ_2 (along $\langle 11\bar{2} \rangle$ axes). These arrangements are indistinguishable by NPD and both result in $0.634(5) \mu_B/\text{Yb}$ ordered moment at 0.45 K in zero field, which is close to $0.77(1) \mu_B/\text{Yb}$ reported by Dalmas de Reotier *et al.*¹⁴ This value is significantly lower than the single-ion expectation value of $1.37 \mu_B$ for the GS doublet and μ_{eff} in the LT regime extracted from susceptibility suggesting strong quantum fluctuations.

To understand the microscopic picture at higher fields we performed Rietveld refinements of difference patterns between data measured at a given magnetic field at 0.45 K and data measured at zero field at 2.5 K. Firstly the isotropic powder averaging was considered. Already at $B=0.5$ T we can fit the pattern by a mixture of the Γ_5 ψ_2/ψ_3 and the Γ_9 IRRs with the basis vectors ψ_7 and ψ_8 , which suggests a crossover between these two states. While the ψ_8 BV corresponds to the ferromagnetic (F) component along the $\langle 001 \rangle$ axis, the ψ_7 BV corresponds to the antiferromagnetic (AF) arrangement along the $\langle 110 \rangle$ axes. This is the so-called ice-like- splayed ferromagnet (SF) observed with the $\langle 111 \rangle$ local axes reported for $\text{Tb}_2\text{Sn}_2\text{O}_7$.²⁴ With increasing field the Γ_5 contribution diminishes and completely vanishes at 3 T, while both Γ_9 components increase with field.

The fits get worse above 3 T because magnetic field aligns the ferromagnetic Γ_9 component and isotropic powder averaging cannot be applied anymore. We approximated this grain alignment by the preferred orientation model using a modified March's function ($(G \cos \alpha)^2 + \frac{\sin^2 \alpha}{G}$)^{-3/2}. Here $G=T_{\perp}/T_{\parallel}$ is a ratio of texture coefficients perpendicular and parallel to the texture vector \mathbf{t} chosen along the F-component $\langle 001 \rangle$, α is the acute angle between the scattering vector \mathbf{Q} and \mathbf{t} . This way we improve the fits significantly. The

obtained values are sensible and the ψ_7 and ψ_8 BVs of Γ_9 match the observed intensities. Still this model needs further corroboration by single crystal neutron diffraction.

For our refined model in the maximum applied field of 5 T the F ψ_8 component is $0.94(1) \mu_B/\text{Yb}$, which is comparable to the net magnetization $0.796 \mu_B/\text{Yb}$ measured for the bulk sample at 0.5 K and 5 T. Summing the F ψ_8 ($0.796 \mu_B/\text{Yb}$) and the AF ψ_7 ($1.26(6) \mu_B/\text{Yb}$) components gives the total ordered moment of $1.58(8) \mu_B/\text{Yb}$, which is comparable to the expected moment $1.37 \mu_B$ of the GS doublet. The obtained value suggests that the fluctuating part of the moment is suppressed as the magnetic field becomes large, as expected.

TABLE II. Magnetic arrangement on the neighbouring Yb-sites 1-4 with the coordinates xyz forming a tetrahedron. From powder neutron diffraction at 0.45 K the moment components are $|M_x|=|M_y|=0.634(5) \mu_B/\text{Yb}$ for B=0 T and $|M_x|=|M_y|=0.900(6) \mu_B/\text{Yb}$, $M_z=0.91(1) \mu_B/\text{Yb}$ for B=5 T.

Site	xyz	B=0 T ψ_2/ψ_3 of Γ_5		B=5 T Γ_9		
		$\psi_2 M_x$	$\psi_2 M_y$	$\psi_7 M_x$	$\psi_7 M_y$	$\psi_8 M_z$
1	$\frac{1}{2} \frac{1}{2} \frac{1}{2}$	+	-	+	+	+
2	$\frac{1}{2} \frac{1}{4} \frac{1}{4}$	+	+	-	+	+
3	$\frac{1}{4} \frac{1}{2} \frac{1}{4}$	-	-	+	-	+
4	$\frac{1}{4} \frac{1}{4} \frac{1}{2}$	-	+	-	-	+

2. Exchange model and comparison to the experiment

To model CdYb_2Se_4 , recall the nearest-neighbour anisotropic exchange model for effective $S = 1/2$ Kramers doublets on the pyrochlore lattice^{25,26}. In terms of the pseudo-spin quantized in the *global* frame this can be written as^{3,26}

$$H = \sum_{\langle ij \rangle} \mathbf{S}_i^\top \mathbf{J}_{ij} \mathbf{S}_j - \mu_B \mathbf{B} \cdot \sum_i \mathbf{g}_i \mathbf{S}_i \quad (2)$$

where \mathbf{J}_{ab} denotes the exchange matrix between sublattices a and b defined as

$$\begin{aligned} \mathbf{J}_{12} &= \begin{pmatrix} J + K + \frac{D}{\sqrt{2}} + \frac{D}{\sqrt{2}} & & \\ -\frac{D}{\sqrt{2}} & J & \Gamma \\ -\frac{D}{\sqrt{2}} & \Gamma & J \end{pmatrix}, & \mathbf{J}_{13} &= \begin{pmatrix} J & -\frac{D}{\sqrt{2}} & \Gamma \\ +\frac{D}{\sqrt{2}} & J + K & +\frac{D}{\sqrt{2}} \\ \Gamma & -\frac{D}{\sqrt{2}} & J \end{pmatrix}, \\ \mathbf{J}_{14} &= \begin{pmatrix} J & \Gamma & -\frac{D}{\sqrt{2}} \\ \Gamma & J & -\frac{D}{\sqrt{2}} \\ +\frac{D}{\sqrt{2}} & +\frac{D}{\sqrt{2}} & J + K \end{pmatrix}, & \mathbf{J}_{23} &= \begin{pmatrix} J & -\Gamma & +\frac{D}{\sqrt{2}} \\ -\Gamma & J & -\frac{D}{\sqrt{2}} \\ -\frac{D}{\sqrt{2}} & +\frac{D}{\sqrt{2}} & J + K \end{pmatrix}, \\ \mathbf{J}_{24} &= \begin{pmatrix} J & +\frac{D}{\sqrt{2}} & -\Gamma \\ -\frac{D}{\sqrt{2}} & J + K & +\frac{D}{\sqrt{2}} \\ -\Gamma & -\frac{D}{\sqrt{2}} & J \end{pmatrix}, & \mathbf{J}_{34} &= \begin{pmatrix} J + K & -\frac{D}{\sqrt{2}} & +\frac{D}{\sqrt{2}} \\ +\frac{D}{\sqrt{2}} & J & -\Gamma \\ -\frac{D}{\sqrt{2}} & -\Gamma & J \end{pmatrix}. \end{aligned}$$

The g -factor matrices, \mathbf{g}_i , are given as

$$\mathbf{g}_i = g_{\pm} (\hat{\mathbf{x}}_i \hat{\mathbf{x}}_i^{\top} + \hat{\mathbf{y}}_i \hat{\mathbf{y}}_i^{\top}) + g_z \hat{\mathbf{z}}_i \hat{\mathbf{z}}_i^{\top}, \quad (3)$$

where $(\hat{\mathbf{x}}_i, \hat{\mathbf{y}}_i, \hat{\mathbf{z}}_i)$ define the local coordinate axes^{3,26}. In this basis there are four exchanges: the isotropic Heisenberg exchange (J), the Kitaev exchange (K), the symmetric off-diagonal exchange (Γ) and the anti-symmetric Dzyaloshinskii-Moriya (DM) exchange (D).

Using theoretical framework of Ref. 8 we expect the exchange parameters of CdYb_2Se_4 to lie in the regime of dominant antiferromagnetic Heisenberg exchange $J > 0$, with subdominant indirect DM, $D < 0$, and small symmetric exchanges K and Γ – that is we expect that $J \gtrsim |D| \gg K, \Gamma$. This scenario puts CdYb_2Se_4 close to the phase boundary between the Γ_5 states and the nearby (splayed) ferromagnet phase. Since the g -factors and CEF ground doublet composition from INS data for CdYb_2Se_4 are not unambiguous, we cannot perform reliable super-exchange calculations, as has been done in Ref. 8. We do note however, that using the g -factors presented in Sec. IV, we find that the values from super-exchange calculations lie precisely in the regime described above.

To determine the exchanges we thus turn to the experimental data. From the Curie-Weiss temperature we can infer the dominant Heisenberg exchange is roughly $J \sim 7$ K. Since a Γ_5 ground state is found experimentally, we assume that $(K + \Gamma) < 0$ and thus such a state is chosen at the classical level. To determine the subdominant (indirect) DM interaction, we consider its effect on the excitation spectrum of the Γ_5 ground states. We find that the position of the intensity maximum (as seen experimentally) corresponds to a flat band that

is directly tuned by the strength of the DM interaction. From this observation, we find that a DM interaction of $D/J \sim -0.3$ best reproduces the zero-field experimental inelastic spectrum (the precise values of K and Γ do not strongly affect this conclusion).

Determining the values of K and Γ is more difficult. We have fixed $K = \Gamma$ and tuned this common value to capture qualitatively the field dependence of the magnetic Bragg intensities; specifically the matching of the field dependence of the upturns in the [200] and [111] intensities. From these considerations we choose $K/J = \Gamma/J = -0.07$, not too far from what has been found via theoretical calculations³, as well as experimentally in a related breathing pyrochlore material¹⁷. Our model is thus

$$K/J = -0.07, \quad \Gamma/J = -0.07, \quad D/J = -0.3, \quad (4)$$

where $J \sim 7$ K. At zero field the model results in the Γ_5 ground state, as is obtained in the experiment. Like in $\text{Yb}_2\text{Ti}_2\text{O}_7$, these exchanges are close to the phase boundary between the SF and Γ_5 phases, suggesting an important role of the competition between these phases in CdYb_2Se_4 . Linear spin-wave theory (LSWT) predicts that quantum fluctuations would select the ψ_3 state out of this manifold through order-by-quantum-disorder^{27,28}, similar to what has been suggested for $\text{Yb}_2\text{Ge}_2\text{O}_7$.

To compare the model and experimental results in an applied magnetic field (both diffraction and inelastic neutron scattering) we emulate the powder averaging, as well the particular neutron scattering geometry, where the collected wave-vectors lie roughly in the plane perpendicular to the field. This results in a correlated average over field orientation and wave-vector $\sim \int d\hat{\mathbf{B}} \int_{\hat{\mathbf{Q}} \perp \hat{\mathbf{B}}} d\hat{\mathbf{Q}}$ for both quantities.

To be explicit, for the magnetic Bragg peaks we consider

$$I(\mathbf{Q}; \mathbf{B}) \propto F(\mathbf{Q})^2 \sum_{\mu\nu} (\delta_{\mu\nu} - \hat{Q}_\mu \hat{Q}_\nu) M_{\mathbf{Q}}^\mu(\mathbf{B})^* M_{\mathbf{Q}}^\nu(\mathbf{B}) \quad (5)$$

where $\mathbf{M}_{\mathbf{Q}}(\mathbf{B}) \equiv \sum_r e^{i\mathbf{Q}\cdot\mathbf{r}} \mathbf{M}_r(\mathbf{B})$ are the Fourier transforms of the classical ground states for a given field \mathbf{B} and $F(\mathbf{Q})$ is the Yb^{3+} magnetic form factor in the dipole approximation. To compare intensities of different peaks in powder patterns the Lorentz factor applied.

For the inelastic spectrum we compute

$$I(\mathbf{Q}, \omega; \mathbf{B}) \propto F(\mathbf{Q})^2 \sum_{\mu\nu} (\delta_{\mu\nu} - \hat{Q}_\mu \hat{Q}_\nu) S_{\mu\nu}(\mathbf{Q}, \omega; \mathbf{B}), \quad (6)$$

where $S_{\mu\nu}(\mathbf{Q}, \omega; \mathbf{B})$ is the dynamical structure factor in a magnetic field \mathbf{B} . We compute this quantity within LSWT, optimizing for a new classical ground state (assuming the expected

$\mathbf{k}=0$ structure) for each field \mathbf{B} considered (direction and magnitude). Accounting for the powder averaging gives

$$I(Q, \omega; B) \propto \int d\hat{\mathbf{B}} \int_{\hat{\mathbf{Q}} \perp \hat{\mathbf{B}}} d\hat{\mathbf{Q}} I(Q\hat{\mathbf{Q}}, \omega; B\hat{\mathbf{B}}), \quad (7)$$

with a similar expression for the Bragg peak intensity

$$I_0(Q; B) \propto \int d\hat{\mathbf{B}} \int_{\hat{\mathbf{Q}} \perp \hat{\mathbf{B}}} d\hat{\mathbf{Q}} I_0(Q\hat{\mathbf{Q}}; B\hat{\mathbf{B}}). \quad (8)$$

At zero-field we consider the expected ψ_3 ground state, averaging over its six domains, though we note that it is difficult to distinguish ψ_3 from the ψ_2 states or a simple average over the Γ_5 manifold.

We show the associated evolution of the magnetic Bragg peaks in Fig. 6 (right). The qualitative features of the Bragg evolution are captured by the theoretical calculation. In particular, one can identify a crossover near 2 – 3 T where the correlations change from antiferromagnetic to ferromagnetic. The evolution of these peaks is qualitatively different from what is observed in other Γ_5 ordered magnets, such as $\text{Er}_2\text{Ti}_2\text{O}_7$; this is a consequence of *Ising*-like g -factors of the GS doublet in TYb_2X_4 ($g_z > g_{\pm}$), compared to the *XY*-like g -factors ($g_z < g_{\pm}$) found in $\text{Er}_2\text{Ti}_2\text{O}_7$. Some details, such as the range of the crossover field or evolution of relative intensity of the peaks, are sensitive to the precise values of the g -factors, and the small symmetric anisotropies K and Γ . Since these quantities are not presently known precisely, a quantitative agreement between theory and experiment should not be expected.

We note that the agreement of the absolute ratios of the intensities at low-fields is not captured by the simple classical calculations. This is likely related to the strong reduction of the ordered moment observed at zero-field, similar to what has been reported in the $\text{Yb}_2\text{B}_2\text{O}_7$ compounds ($\text{B} = \text{Ti}, \text{Sn}$ and Ge). This reduction could be related to quantum fluctuations and frustration and should thus be relieved as the magnetic field is increased, as is observed. When determining the ratios $K/J = \Gamma/J = -0.07$ we thus focused on the high-field values and the field dependence of the intensities, ignoring inconsistencies in the overall relative intensities that appear at low field (vs. high-field).

We discuss now the inelastic spectrum shown in Figs. 7. To facilitate comparison of the calculated spectra with the experimental data, we have included a Gaussian broadening to emulate the finite experimental resolution (middle panel). The spectra contain a broad

maximum near $Q \sim 1 \text{ \AA}$ and $\omega \sim 0.7 \text{ meV}$ (used to fix $D/J = -0.3$) which matches well the experimental spectra presented in Fig. 7 (left panel). Note that the overall bandwidth of these excitations at zero-field is set by the overall scale J , giving a cross-check on the exchange scale determined from the Curie-Weiss fit.

The sharper features present in the INS spectrum at zero field persist to fields of order 2 – 3 T and then start to dissipate. At larger fields the spin-waves quickly lose intensity as they spread out over a large energy range. This is qualitatively consistent with the experimental data. It can be understood as a consequence of the magnetic anisotropy of this system, in both the single-ion properties and the exchange interactions, causing the excitation spectrum to depend strongly on the field direction. The powder averaging thus produces a variety of quite different spectra that, when averaged, become diffuse without any distinctive feature in the range of wave-vectors probed.

V. OUTLOOK

Summarising our findings we find that the CdYb_2Se_4 spinel shows strong similarities to the ytterbium pyrochlore oxides $\text{Yb}_2\text{B}_2\text{O}_7$ ($R = \text{Yb, Er}$ and $B = \text{Sn, Ti, Ge}$). It is worth mentioning that XY pyrochlore magnets have a remarkably rich phase diagram²⁹, with several competing $\mathbf{k}=0$ magnetic orders, such as the Palmer-Chalker states, the Γ_5 manifold with noncoplanar ψ_2 and collinear ψ_3 states, and splayed ice-like and XY -like ferromagnets. The zero field ordered state in CdYb_2Se_4 , similarly to $\text{Er}_2\text{Ti}_2\text{O}_7$, $\text{Er}_2\text{Ge}_2\text{O}_7$ and $\text{Yb}_2\text{Ge}_2\text{O}_7$, belongs to the Γ_5 irreducible representation. In this Γ_5 manifold the classical degeneracy between these states can be lifted by several different competing order-by-disorder mechanisms, such as thermal-, quantum-, structural- or virtual-crystal-field-fluctuations.^{3,15,27,28,30–32} From our powder diffraction data we cannot distinguish between the expected selection of ψ_2 or ψ_3 states, though our calculations suggest a ψ_3 ground state for CdYb_2Se_4 .

Identification of the selected state from the Γ_5 manifold is difficult. In $\text{Er}_2\text{Ti}_2\text{O}_7$ theoretical predictions, based on exchanges determined at high fields, and the experimental ground state agree^{28,29,33,34}, with the ψ_2 ground state chosen. This selection manifests in single crystal neutron diffraction³⁴ and in the behavior under small magnetic fields,³³ as well as in more indirect probes such as the opening of a small pseudo-Goldstone gap^{35,36}. Definite

identification of the ordered state in CdYb_2Se_4 requires experiments on single crystals.

More direct parallels can be drawn to the ytterbium pyrochlores. The germanate $\text{Yb}_2\text{Ge}_2\text{O}_7$ seems to be the closest analogue to the CdYb_2Se_4 spinel, though given the limited information available on this compound, we focus our attention on $\text{Yb}_2\text{Ti}_2\text{O}_7$, which has been more extensively studied.³⁷⁻⁴¹ In $\text{Yb}_2\text{Ti}_2\text{O}_7$ the ground state was long disputed, due to sample-to-sample variations in experimental properties. The present consensus is that the ground state of $\text{Yb}_2\text{Ti}_2\text{O}_7$ is a splayed ice-like ferromagnet. Mysteries still remain however, such as in the diffuse rods of scattering along the $\langle 111 \rangle$ directions above T_C , and in the absence of well defined spin waves at zero field³⁷. The origin of the short-range correlations giving rise to rods can be partly understood as a result of proximity of $\text{Yb}_2\text{Ti}_2\text{O}_7$ to the Γ_5 phase boundary^{42,43}, while a complete understanding of the magnetic excitations is still missing. Open questions include the role of strong quantum fluctuations and the importance of extrinsic effects such as disorder play in determining the magnetic spectrum.

Given the CdYb_2Se_4 spinel appears to be located in the same interesting region of the phase diagram that has driven interest in the $\text{Yb}_2\text{B}_2\text{O}_7$ pyrochlores, one might hope that, given its different crystal structure, it may shed some light on the outstanding issues in these compounds. Research in pyrochlore magnets distinct from the rare-earth pyrochlore oxides already proved to be very useful in related compounds. For example, in the dipolar spin ice state of the CdEr_2Se_4 spinel,¹² the monopole dynamics appears to be much faster than in the canonical spin ice $\text{Dy}_2\text{Ti}_2\text{O}_7$ and thus it can bring insight into processes which require equilibration at much lower temperatures that pyrochlore titanates allow.

VI. CONCLUSIONS

Our experimental findings and theoretical modelling reveal that low-temperature magnetic properties of the CdYb_2Se_4 spinel are dominated by the well-isolated ytterbium ground state doublet with effective spin $S = 1/2$. The CEF analysis, combined with the evolution of the magnetic structure in field, suggests a weak Ising character of the ytterbium ground state doublet. Nevertheless the anisotropic exchange interactions of CdYb_2Se_4 select a ground state of the XY -type, with long-range antiferromagnetic Γ_5 order below $T_N = 1.8$ K. Through comparison of the inelastic spectrum with theoretical models, we find that the properties of CdYb_2Se_4 are consistent with expectations that it lies close to the phase

boundary between the Γ_5 states and an SF phase, similar to the $\text{Yb}_2\text{B}_2\text{O}_7$ pyrochlores. Further growth of single crystals of the CdYb_2Se_4 spinel will allow to explore this physics, and test the universality of some of the more exotic features (such as the broad continuum of excitations) that have been observed in other ytterbium pyrochlores.

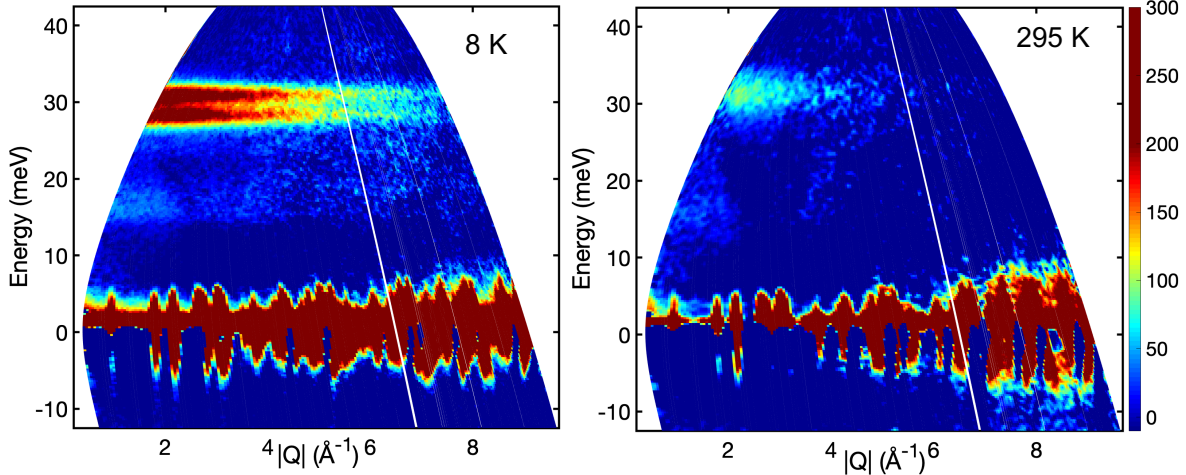


FIG. 1. High-energy inelastic neutron scattering spectra at 8 K (left) and 295 K (right) measured on the MERLIN spectrometer with $E_i = 50$ meV.

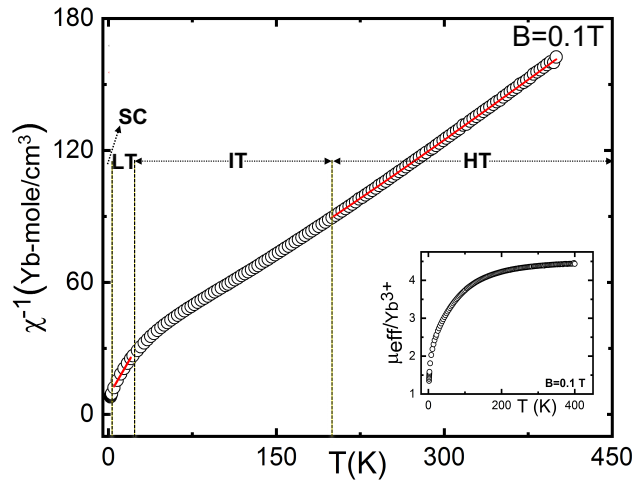


FIG. 2. Inverse susceptibility $1/\chi$ in the four regimes measured at $B=0.1$ T and (insert) effective moment μ_{eff} versus temperature. The red solid lines are the linear Curie-Weiss fits.

ACKNOWLEDGMENTS

This work was performed at SINQ, Paul Scherrer Institute, Villigen, Switzerland with financial support of the Swiss National Science Foundation (SNF) (Grant No. 200021-140862). This work was in part supported by Deutsche Forschungsgemeinschaft (DFG) (Grant SFB 1143) and SNF (Grant No. 206021-139082). We thank S. Gao, M. Pregelj, M.

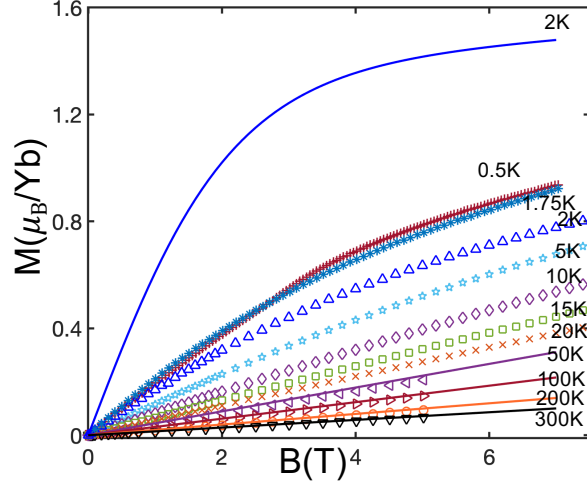


FIG. 3. Field dependence of the isothermal magnetization. Experimental data are shown by symbols. The solid lines represent calculated²³ magnetization in the HT regime and at 2 K.

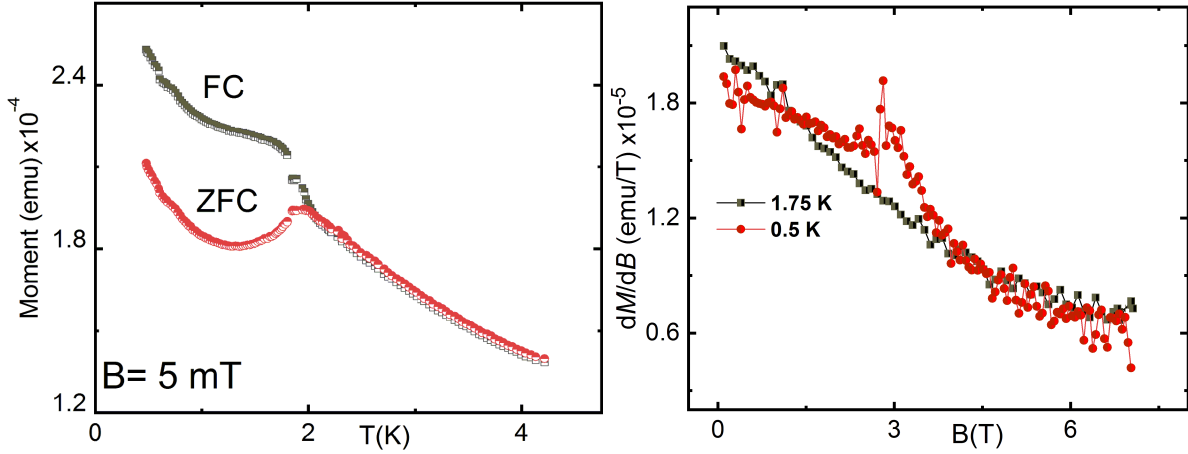


FIG. 4. Left: Magnetization for the sample cooled in zero field (ZFC) (red symbols) and in an applied magnetic field (FC) $B= 5$ mT (black symbols). Right: Magnetic field derivative of the isothermal magnetization dM/dB at $T=0.5$ K (red symbols) and $T=1.75$ K (black symbols).

J. P. Gingras for discussions.

* oksana.zaharko@psi.ch

¹ J. S. Gardner, M. J. P. Gingras, J. E. Greedan, Rev. Mod. Phys. **82**, 53 (2010).

² A. M. Hallas, J. Gaudet, B. D. Gaulin, Annu. Rev. Condens. Matter Phys **9**, 105 (2018).

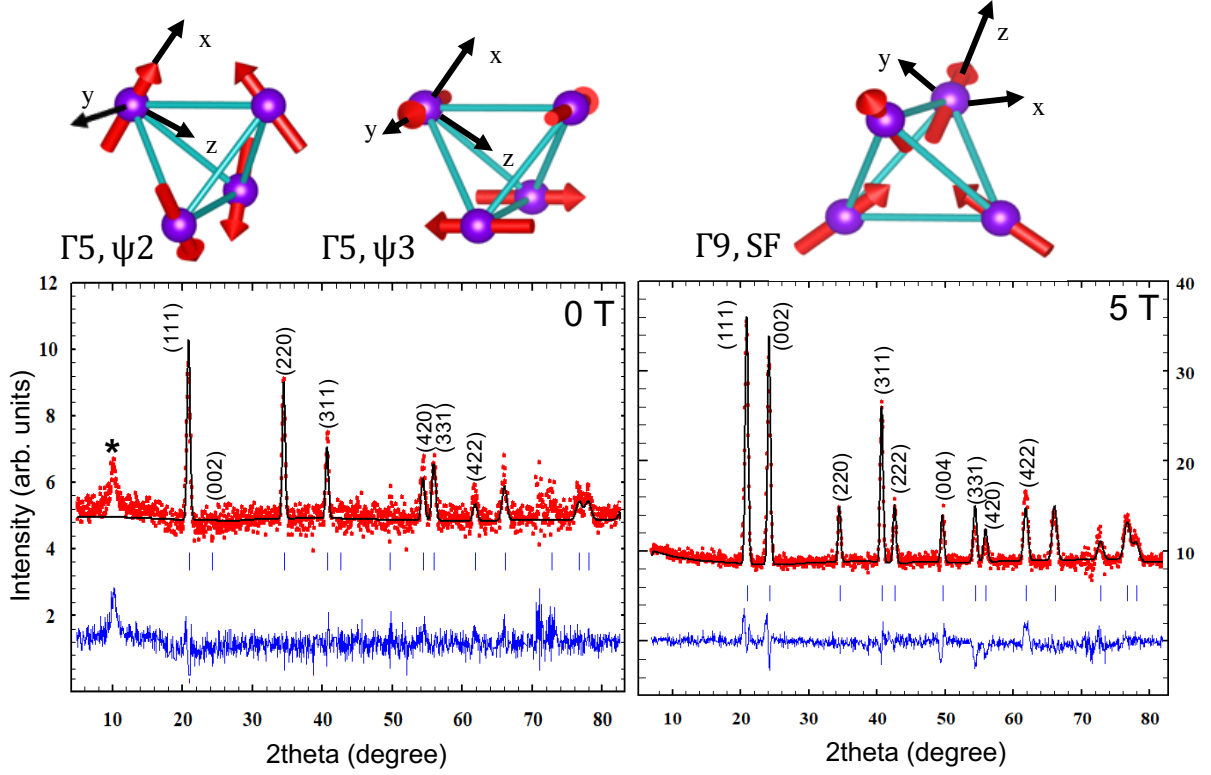


FIG. 5. Top: Magnetic moment arrangements for the ψ_2 and ψ_3 states of Γ_5 and the splayed Γ_9 ferromagnet. Bottom: 0.45 K-2.5 K observed, calculated and difference neutron diffraction patterns at 0 T (left) and 5 T (right). The vertical markers designate the $\mathbf{k}=0$ reflections. The broad peak at $2\theta=10$ deg is an impurity.²²

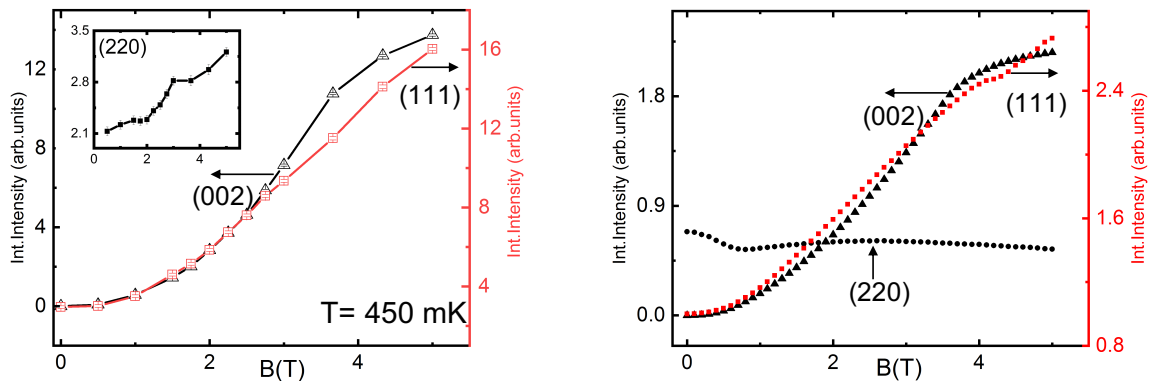


FIG. 6. Evolution of the magnetic Bragg peaks (002), (111) and (220) in applied magnetic field in neutron diffraction patterns (left) and according to our theoretical model (right).

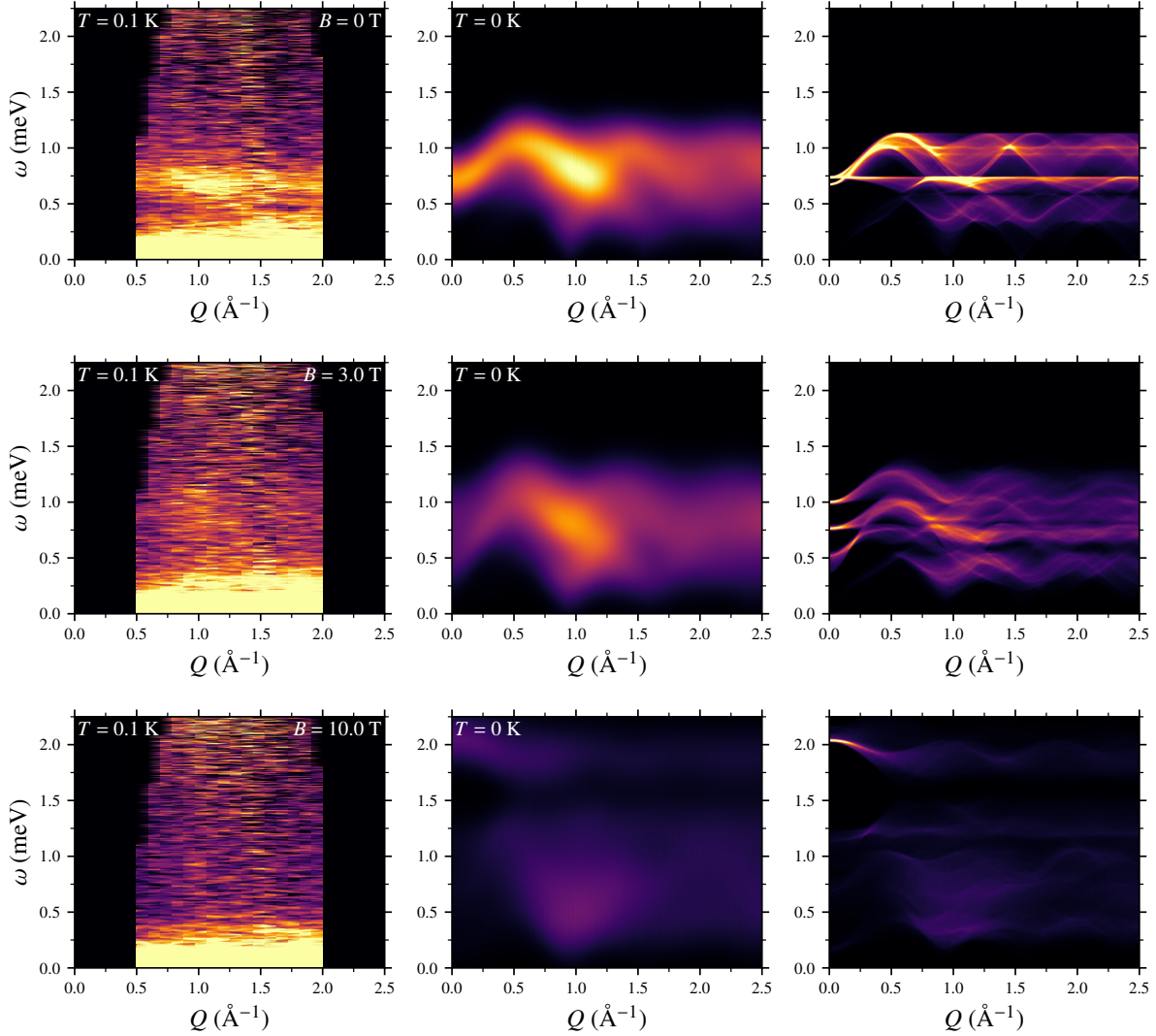


FIG. 7. Low-energy excitation spectrum of CdYb_2Se_4 at $B=0$ T (top), 3 T (middle), 10 T (bottom). Left: inelastic neutron scattering measured on FOCUS with $E_i=3.7$ meV at $T=0.1$ K. Right: INS for our model with the exchange parameters of CdYb_2Se_4 computed within linear spin-wave theory at $T=0$ K. The powder average only includes $\hat{Q} \perp \hat{B}$ for each randomly sampled \hat{B} , as given in Eq. (7). Middle: Calculated spectra from the right panel broadened to better match the experimental resolution.

³ J. G. Rau, M. J. P. Gingras, *Annu. Rev. Condens. Matter Phys* **10**, 357 (2019).

⁴ S.T. Bramwell and M. J. Gingras, *Science* **294**, 1495 (2001).

⁵ R. Sibille, N. Gauthier, H. Yan, M.-C. Hatnean, J. Ollivier, B. Winn, U. Filges, G. Balakrishnan, M. Kenzelmann, N. Shannon, T. Fennell, *Nature Physics* **14**, 711 (2018).

- ⁶ J. Gaudet, E. M. Smith, J. Dudemaine, J. Beare, C. R. C. Buhariwalla, N. P. Butch, M. B. Stone, A. I. Kolesnikov, G. Xu, D. R. Yahne, K. A. Ross, C. A. Marjerrison, J. D. Garrett, G. M. Luke, A. D. Bianchi, B. D. Gaulin, *Phys. Rev. Lett.* **122**, 187201 (2019).
- ⁷ M. J. P. Gingras, P. A. McClarty, *Rep. Prog. Phys.* **77**, 056501 (2014).
- ⁸ J. G. Rau, M. J. P. Gingras, *Phys. Rev. B* **98**, 054408 (2018).
- ⁹ G. C. Lau, R. S. Freitas, B. G. Ueland, P. Schiffer, R. J. Cava, *Phys. Rev. B* **72**, 054411 (2005).
- ¹⁰ J. D. M. Champion, M. J. Harris, P. C. W. Holdsworth, A. S. Wills, G. Balakrishnan, S. T. Bramwell, E. Čížmár, T. Fennell, J. S. Gardner, J. Lago, D. F. McMorrow, M. Orendáč, A. Orendáčová, D. McK. Paul, R. I. Smith, M. T. F. Telling, and A. Wildes, *Phys. Rev. B* **68**, 020401(R) (2003).
- ¹¹ J. Lago, I. Živković, B. Z. Malkin, J. R. Fernandez, P. Ghigna, P. Dalmas de Réotier, A. Yaouanc, T. Rojo *Phys. Rev. Lett.* **104**, 247203 (2010).
- ¹² S. Gao, O. Zaharko, V. Tsurkan, L. Prodan, E. Riordan, J. Lago, B. Fåk, A. R. Wildes, M. M. Koza, C. Ritter, P. Fouquet, L. Keller, E. Canévet, M. Medarde, J. Blomgren, C. Johansson, S. R. Giblin, S. Vrtnik, J. Luzar, A. Loidl, C. Rüegg, T. Fennell, *Phys. Rev. Lett.* **120**, 137201 (2018).
- ¹³ T. Higo, K. Iritani, M. Halim, W. Higemoto, T. U. Ito, K. Kuga, K. Kimura, S. Nakatsuji, *Phys. Rev. B* **95**, 174443 (2017).
- ¹⁴ P. Dalmas de Réotier, C. Marin, A. Yaouanc, C. Ritter, A. Maisuradze, B. Roessli, A. Bertin, P. J. Baker, A. Amato, *Phys. Rev. B* **96**, 134403 (2017).
- ¹⁵ J. G. Rau, S. Petit, M. J. P. Gingras, *Phys. Rev. B* **93**, 184408 (2016).
- ¹⁶ The possible magnetic orders on the pyrochlore lattice are summarised in numerous publications, see for example Refs. 2, 3, and 14.
- ¹⁷ J. G. Rau, L. S. Wu, A. F. May, L. Poudel, B. Winn, V. O. Garlea, A. Huq, P. Whitfield, A. E. Taylor, M. D. Lumsden, M. J. P. Gingras, A. D. Christianson, *Phys. Rev. Lett.* **116**, 257204 (2016).
- ¹⁸ R. I. Bewley, T. Guidi, S. M. Bennington, *Notiziario Neutroni e Luce di Sincrotrone* **14**, 22 (2009).
- ¹⁹ M. Rotter, *J. Mag. Magn. Mater.* 272-276, E481 (2004).
- ²⁰ J. Rodríguez-Carvajal, *Phys. B: Condens. Matt.* **192**, 55 (1993).
- ²¹ O. Petrenko, M. R. Lees, G. Balakrishnan, *Eur. Phys. J. B* **86**, 416 (2013).

- ²² We observed also an additional peak which can be indexed as $(\frac{1}{2} \frac{1}{2} \frac{1}{2})$ of CdYb_2Se_4 . Réotier *et al.*¹⁴ attributed it to an impurity. Indeed, this is probably the $(0 \ 0 \ \frac{1}{2})$ magnetic peak of $\text{Yb}_2\text{O}_2\text{Se}$, which orders at $T_N=2.65$ K with the wave vector $(0 \ 0 \ \frac{1}{2})$.
- ²³ D. Le SAfiCF. URL <http://www.yocto.me/work/saficf/index.html>
- ²⁴ I. Mirebeau, A. Apetrei, J. Rodríguez-Carvajal, P. Bonville, A. Forget, D. Colson, V. Glazkov, J. P. Sanchez, O. Isnard, E. Suard, Phys. Rev. Lett. **94**, 246402 (2005).
- ²⁵ S. H. Curnoe, Phys. Rev. B **78**, 094418 (2008).
- ²⁶ K. A. Ross, L. Savary, B.D. Gaulin, L. Balents, Phys. Rev. X **1**, 1021002 (2011).
- ²⁷ M. E. Zhitomirsky, M.V. Gvozdikova, P. C.W. Holdsworth, R. Moessner, Phys. Rev. Lett. **109**, 077204 (2012).
- ²⁸ L. Savary, K. A. Ross, B. D. Gaulin, J. P. C. Ruff, L. Balents, Phys. Rev. Lett. **109**, 167201 (2012).
- ²⁹ A. W. C. Wong, Z. Hao, M. J. P. Gingras, Phys. Rev. B **88**, 144402 (2013).
- ³⁰ P. A. McClarty, P. Stasiak, M. J. P. Gingras, Phys. Rev. B **89**, 024425 (2014).
- ³¹ A. Andreev, P. A. McClarty, Phys. Rev. B **91**, 064401 (2015).
- ³² V. S. Maryasin and M. E. Zhitomirsky, Phys. Rev. B **90**, 094412 (2014).
- ³³ E. Lhotel, J. Robert, E. Ressouche, F. Damay, I. Mirebeau, J. Ollivier, H. Mutka, P. Dalmas de Réotier, A. Yaouanc, C. Marin, C. Decorse, S. Petit, Phys. Rev. B **95**, 134426 (2017).
- ³⁴ A. Poole, A. S. Wills, E. Lelièvre-Berna, J. Phys. : Condens. Matt. **19**, 452201 (2007).
- ³⁵ K. A. Ross, Y. Qiu, J. R. D. Copley, H. A. Dabkowska, B. D. Gaulin, Phys. Rev. Lett. **112**, 057201 (2014).
- ³⁶ S. Petit, J. Robert, S. Guitteny, P. Bonville, C. Decorse, J. Ollivier, H. Mutka, M. J. P. Gingras, I. Mirebeau, Phys. Rev. B **90**, 060410(R) (2014).
- ³⁷ J. D. Thompson, P. A. McClarty, D. Prabhakaran, I. Cabrera, T. Guidi, R. Coldea, Phys. Rev. Lett. **119**, 057203 (2017).
- ³⁸ K. A. Ross, J. P. C. Ruff, C. P. Adams, J. S. Gardner, H. A. Dabkowska, Y. Qiu, J. R. D. Copley, B. D. Gaulin, Phys. Rev. Lett. **103**, 227202 (2009).
- ³⁹ L.-J. Chang, S. Onoda, Y. Su, Y.-J. Kao, K.-D. Tsuei, Y. Yasui, K. Kakurai, M. R. Lees, Nature Comm. **3**, 992 (2012).
- ⁴⁰ J. Robert, E. Lhotel, G. Remenyi, S. Sahling, I. Mirebeau, C. Decorse, B. Canals, S. Petit, Phys. Rev. B **92**, 064425 (2015).

- ⁴¹ J. Gaudet, K. A. Ross, E. Kermarrec, N. P. Butch, G. Ehlers, H. A. Dabkowska, B. D. Gaulin, *Phys. Rev. B* **93**, 064406 (2016).
- ⁴² H. Yan, O. Benton, L. Jaubert, N. Shannon, *Phys. Rev. B* **95**, 094422 (2017).
- ⁴³ L. Jaubert, O. Benton, J. G. Rau, J. Oitmaa, R. R. P. Singh, N. Shannon, M. J. P. Gingras, *Phys. Rev. Lett.* **115**, 267208 (2015).
- ⁴⁴ A. Yaouanc, P. Dalmas de Réotier, L. Keller, B. Roessli, A. Forget, *J. Phys.: Condens. Matter.* **28**, 426002 (2016).
- ⁴⁵ A. M. Hallas, J. Gaudet, N. P. Butch, M. Tachibana, R. S. Freitas, G. M. Luke, C. R. Wiebe, B. D. Gaulin, *Phys. Rev. B* **93**, 100403(R) (2016).